JVI Journals.ASM.org

Structure of the Fusion Core and Inhibition of Fusion by a Heptad Repeat Peptide Derived from the S Protein of Middle East Respiratory Syndrome Coronavirus

Jing Gao,[a,b] Guangwen Lu,[a] Jianxun Qi,[a] Yan Li,[a] Ying Wu,[a] Yao Deng,[c] Heyuan Geng,[c] Hongbin Li,[d] Qihui Wang,[a] Haixia Xiao,[e] Wenjie Tan,[c] Jinghua Yan,[a] George F. Gao[a,b,e,f,g]

CAS Key Laboratory of Pathogenic Microbiology and Immunology, Institute of Microbiology, Chinese Academy of Sciences, Beijing, China[a]; University of Chinese Academy of Sciences, Beijing, China[b]; Biotech Center for Viral Disease Emergency, Institute for Viral Disease Control and Prevention, Chinese Center for Disease Control and Prevention (China CDC), Beijing, China[c]; Core Facility, Institute of Microbiology, Chinese Academy of Sciences, Beijing, China[d]; Laboratory of Protein Engineering and Vaccines, Tianjin Institute of Industrial Biotechnology, Chinese Academy of Sciences, Tianjin, China[e]; Research Network of Immunity and Health (RNIH), Beijing Institutes of Life Science, Chinese Academy of Sciences, Beijing, China[f]; Office of Director-General, Chinese Center for Disease Control and Prevention (China CDC), Beijing, China[g]

Middle East respiratory syndrome coronavirus (MERS-CoV) recently emerged as a severe worldwide public health concern. The virus is highly pathogenic, manifesting in infected patients with an approximately 50% fatality rate. It is known that the surface spike (S) proteins of coronaviruses mediate receptor recognition and membrane fusion, thereby playing an indispensable role in initiating infection. In this process, heptad repeats 1 and 2 (HR1 and HR2) of the S protein assemble into a complex called the fusion core, which represents a key membrane fusion architecture. To date, however, the MERS-CoV fusion core remains uncharacterized. In this study, we performed a series of biochemical and biophysical analyses characterizing the HR1/HR2 complexes of this novel virus. The HR sequences were variably truncated and then connected with a flexible amino acid linker. In each case, the recombinant protein automatically assembled into a trimer in solution, displaying a typical α-helical structure. One of these trimers was successfully crystallized, and its structure was solved at a resolution of 1.9 Å. A canonical 6-helix bundle, like those reported for other coronaviruses, was revealed, with three HR1 helices forming the central coiled-coil core and three HR2 chains surrounding the core in the HR1 side grooves. This demonstrates that MERS-CoV utilizes a mechanism similar to those of other class I enveloped viruses for membrane fusion. With this notion, we further identified an HR2-based peptide that could potently inhibit MERS-CoV fusion and entry by using a pseudotyped-virus system. These results lay the groundwork for future inhibitory peptidic drug design.

The newly emergent Middle East respiratory syndrome coronavirus (MERS-CoV) poses a severe threat to public health worldwide. Clinically, the virus can cause a series of respiratory manifestations, including fever, cough, shortness of breath, and acute respiratory distress syndrome (ARDS) (1, 2). These clinical symptoms are accompanied by a high risk of renal failure, leading to a very high mortality rate. As of 29 July 2013, the World Health Organization (WHO) has reported 91 laboratory-confirmed infection cases by this novel coronavirus, of which 46 patients ultimately died despite intensive clinical treatments (3). This unusual pathogenicity distinguishes MERS-CoV from most other coronaviruses, which only cause mild illness in humans (4), and relates MERS-CoV to the severe acute respiratory syndrome (SARS) coronavirus (SARS-CoV). Thus, the potential for a future MERS-CoV pandemic is undeniable.

To combat a virus, it is necessary to understand its infection process. MERS-CoV is an enveloped virus, meaning that the initiation of infection requires fusion between the viral envelope and the cell membrane of the host (5, 6). This process, according to previous studies of other coronaviruses (7), is mediated by the viral surface spike (S) protein and should involve two separate but related events of virus-host interactions: receptor recognition and subsequent membrane fusion. In host cells, the S protein is normally cleaved into S1 and S2 subunits, which are noncovalently linked and embedded in the viral surface envelope (7). The S1 subunit engages the cellular receptors, mediating attachment of the virus to the cell surface, while the S2 subunit mediates membrane fusion (7). Consistent with this notion, MERS-CoV S is indeed cleaved into S1 and S2 subunits (8). S1 recognizes human dipeptidyl peptidase 4 (DPP4/CD26) as a functional receptor (9). Further, the complex structure of the receptor binding domain in MERS-CoV S1 bound to CD26 has been successfully solved by our group (10), illustrating the molecular basis of receptor recognition by this novel virus. Following receptor binding, fusion occurs, and this is expected to involve rearrangement of the characteristic elements called heptad repeats (HRs) in S2 to form a stable 6-helix bundle fusion core (5).

The HR motifs consist of a group of tandemly arranged seven-residue repeats, where the residue positions are indicated with the lowercase letters a, b, c, d, e, f, and g. In this motif, the amino acids in positions "a" and "d" are predominantly hydrophobic or have bulky side chains (11, 12). This sequence feature has the capacity to generate a hydrophobic interface along an α-helix, enabling the formation of a coiled-coil structural module when several HR-containing polypeptide chains are arranged together in parallel (11, 12). Many viruses utilize this specific HR feature for mem-

Received 23 August 2013 **Accepted** 18 September 2013
Published ahead of print 25 September 2013
Address correspondence to George F. Gao, gaof@im.ac.cn.

doi:10.1128/JVI.02433-13

brane fusion. Indeed, the presence of HR regions in viral surface membrane fusion proteins is considered a characteristic of class I enveloped viruses (5, 6). In coronaviruses, the HR elements in the viral S2 subunit are further denoted HR1 and HR2, with the former normally longer than the latter (13–15). Structurally, HR1 and HR2 of coronaviruses form a fold described as a trimer of hairpins, in which three helical HR1 peptides assemble into a coiled-coil core and the helical HR2 peptides bind to the conserved hydrophobic grooves formed by HR1 (5, 6). This featured 6-helix bundle structure, which is also called the virus fusion core, has been crystallographically described for both murine hepatitis virus (MHV) (15) and SARS-CoV (13).

It is generally believed that a series of conformational changes occur in the coronavirus HR regions during the viral fusion process (16). Under the current paradigm, at least three conformational states are proposed for all class I virus envelope proteins, including a prefusion native state, a prehairpin intermediate state, and a stable postfusion hairpin state (16). The formation of a 6-helix bundle would bring the cellular and viral lipid bilayers into proximity, allowing membrane fusion (16). Therefore, the observed fusion core structure likely represents the postfusion state. Prior to bundle assembling, however, HR1 and HR2 should experience a transient intermediate state in which both units are exposed and accessible. HR2 is hypothesized to be unstructured before binding to HR1, which is believed to be α-helical. This notion is supported by the fact that introduced HR peptides compete with endogenous HR counterparts and thereby prevent virus infection (16). Based on this model, several potent inhibitory peptides have been successfully designed for inhibition of viral infections, such as with human immunodeficiency virus (HIV) (17, 18), Ebola virus (19), and SARS-CoV (14, 20). The same rule is expected to be applicable to MERS-CoV. However, structural and functional data on MERS-CoV HR1 and HR2 are not available to corroborate this.

In this study, we characterized the binding of the two HR regions in MERS-CoV S2 via both biophysical and biochemical methods. The crystal structure of the fusion core was successfully solved, revealing a 6-helix fold similar to those reported for the MHV and SARS-CoV fusion cores. We also identified an HR2-based peptide that potently inhibited pseudotyped virus infection, demonstrating that a similar approach can be used to identify MERS-CoV inhibitors. In addition, the structure also provided important atomic details that will be valuable in structure-based drug design.

MATERIALS AND METHODS

Cell lines. 293T cells (for pseudotyped virus generation) and human hepatoma cells (Huh7; for viral infection assay) were cultured in Dulbecco's modified Eagle's medium (DMEM) supplemented with 10% fetal bovine serum. All cell lines were maintained at 37°C in humidified air containing 5% CO_2.

Gene construction. Two constructs with variably truncated HR1 and HR2 sequences were made: one involves MERS-CoV spike (GenBank accession number JX869059) residues E992 to L1040 for HR1 and I1246 to L1286 for HR2, and the other covers amino acids E992 to I1054 for HR1 and L1252 to L1286 for HR2. The fusion core was then prepared as a single chain by linking the HR1 and HR2 domains via a 22-amino-acid linker (LVPRGSGGSGGSGGLEVLFQGP). This flexible linker has been shown to work successfully in the SARS-CoV fusion core (13). The coding fragments were synthesized by Generay Biotech Co., Ltd., and inserted into the NdeI and XhoI restriction sites of the pET-21a vector. The hexahistidine tag coding sequence and the stop codon in the pET-21a vector were used for both constructs.

The construct used for pseudovirus production was cloned by inserting the full-length coding sequence of MERS-CoV spike into the pCAGGS vector to yield a recombinant plasmid named pCAGGS-MERS-S. The construct was then verified by direct DNA sequencing.

Protein expression and purification. For protein expression, expression vectors were transformed into *Escherichia coli* strain BL21(DE3) competent cells. A single colony was inoculated into 50 ml of Luria-Bertani (LB) medium containing 100 μg/ml of ampicillin and incubated overnight at 37°C. Then, the overnight culture was transferred to 2 liters of fresh LB medium for large-scale protein production by growing at 37°C. When the culture density (optical density at 600 nm [OD_{600}]) reached 0.6, protein overexpression was induced with 0.2 mM isopropyl-β-D-thiogalactoside (IPTG), and the cells were grown for an additional 10 h at 16°C before harvesting via centrifugation.

The collected bacterial cell pellet was resuspended in phosphate-buffered saline (PBS) and homogenized by sonication. The suspension was then centrifuged at 12,000 rpm for 15 min at 4°C. The supernatant was collected and then loaded onto a nickel-nitrilotriacetic acid (Ni-NTA) column (Qiagen). After removal of impurities by thorough washing using PBS, the target protein was eluted with a buffer of 300 mM imidazole in PBS and then purified by gel filtration using a Superdex 200 10/300 GL column (GE) running on an Äkta Explorer fast-performance liquid chromatography (FPLC) system in a buffer composed of 20 mM Tris-HCl, pH 8.0, and 100 mM NaCl. The protein fractions were collected and analyzed on a 15% tricine SDS-PAGE gel. The molecular weights of the peak fractions were estimated by comparison with protein standards run on the same column.

Crystallization, data collection, and structure determination. The purified protein was concentrated to 5 mg/ml. Crystals of good diffracting quality were obtained after 14 days using the sitting drop vapor diffusion method by equilibrating a 2-μl drop (protein solution mixed 1:1 with reservoir solution) against a 100-μl reservoir containing 0.1 M bis-tris, pH 6.5, and 25% (wt/vol) polyethylene glycol 3350. For data collection, a single crystal was picked up using a nylon loop and immersed in a cryoprotectant solution containing 67% reservoir solution and 16% glycerol for ~30 s. The crystal was then remounted and flash-cooled in liquid nitrogen. The diffraction data were collected at 100 K at beamline BL17U of the Shanghai Synchrotron Radiation Facility (SSRF). Raw data were processed using HKL2000 (21).

The structure of the MERS-CoV HR1/HR2 complex was determined by molecular replacement with Phaser (22) using the structure of the SARS-CoV fusion core (Protein Data Bank [PDB] code, 1WNC) as the search model. The initial model was first refined with Refmac5 in the CCP4 suite (23) using rigid-body refinement and maximum likelihood procedures. The model was then completed by iterative cycles of manual rebuilding in coot (24) and refinement with Phenix.refine (25). During the course of model building and refinement, PROCHECK (26) was used to monitor the stereochemistry of the structure. The detailed statistics are summarized in Table 1. All of the structural figures were generated using PyMOL (http://www.pymol.org/).

CD spectroscopy. Circular dichroism (CD) spectra were measured on a ChiraScan CD spectrometer (AppliedPhotophysics). Freshly prepared MERS-CoV HR1/HR2 complex proteins were adjusted to 0.2 mg/ml in PBS before data collection. Wavelength spectra were recorded at 20°C using a 0.1-cm-path-length cuvette. Each scan, in the range of 195 to 260 nm, was obtained by taking data points every 0.5 nm with a bandwidth of 2 nm.

Pseudovirus preparation and titration. The MERS pseudovirus was prepared by cotransfecting 293T cells with a plasmid encoding an Env-defective, luciferase-expressing HIV-1 genome (pNL4-3.luc.RE) (27) and the pCAGGS-MERS-S expression plasmid using Lipofectamine 2000 (Invitrogen). The pseudovirus-containing supernatant was harvested 48 h following transfection, clarified by centrifugation, and then filtered

TABLE 1 Crystallographic data collection and refinement statistics for MERS-CoV fusion core

Parameter	Value[a]
Data collection statistics	
Space group	P3
Cell dimensions	
a, *b*, *c* (Å)	42.82, 42.82, 75.57
α, β, γ (°)	90, 90, 120
Resolution (Å)	50–1.90 (1.97–1.90)
R_{merge}	0.074 (0.156)
$I/\sigma I$	18.4 (11.7)
Completeness (%)	99.3 (100.0)
Redundancy	4.5 (4.9)
Refinement statistics	
Resolution (Å)	37.78–1.90
No. of reflections	12,169
R_{work}/R_{free}	0.1847/0.2135
No. of atoms	
Protein	1,200
Ligand/ion	0
Water	130
B-factors	
Protein	20.4
Ligand/ion	
Water	31.1
RMSD	
Bond lengths (Å)	0.009
Bond angles (°)	1.033
Ramachandran analysis	
Most favored (%)	95.7
Additional allowed (%)	3.6
Generally allowed (%)	0.7
Disallowed (%)	0

[a] Values in parentheses are for the highest-resolution shell.

through a 0.45-μm sterilized membrane. Single-use aliquots (1.0 ml) were stored at −80°C. The 50% tissue culture infectious dose ($TCID_{50}$) for each pseudovirus preparation was determined by infection of Huh7 cells as previously described (28).

Peptide synthesis. The peptides used in this study were synthesized by ChinaPeptides Co., Ltd., with a purity of >95%. Each peptide was dissolved in 100% dimethyl sulfoxide (DMSO) at 100 mM and stored at −80°C before use. One peptide (denoted P1; LTQINTTLLDLTYEMLSLQQVVKALNESYIDLKEL) covers the full length of the HR2 sequence, while the other one (denoted P2; LTYEMLSLQQVVKALNESYIDLKELGN) removes those residues in HR2 adopting extended conformations and includes two extra amino acids at the C terminus because the equivalent peptide in SARS-CoV exhibits a much higher inhibitory efficacy than the HR2 peptides of longer length (29). We also included the SARS-peptide (29) (denoted SARS-pep; IQKEIDRLNEVAKNLNESLIDLQELGK) in the pseudovirus entry inhibition assay as a specificity control.

Pseudovirus entry inhibition assay. For the inhibition assay, 100 $TCID_{50}$s of each pseudovirus was incubated with 10-fold serially diluted peptides from 0.01 nM to 100 μM at 37°C for 30 min. The virus-peptide mixture was then transferred to 96-well plates seeded with Huh7 cells. Each concentration was tested in octuplicate. After a 5-h incubation, the medium was replaced, and the sample was incubated for an additional 48 h at 37°C. The cells were then collected, lysed, and measured for luciferase activity using a GloMax 96 Microplate luminometer (Promega). The 50% effective concentration (EC_{50}) and 95% confidence interval values were calculated using Prism.

Protein structure accession number. The atomic coordinates and the related structure factors have been deposited in the Protein Data Bank with the accession code of 4MOD.

RESULTS

Characterization of the binding between MERS-CoV HR1 and HR2. The HR regions exhibit characteristic sequence features with normally hydrophobic residues at the "a" and "d" positions. With this criterion, we first positioned the HR sequences of MERS-CoV to amino acids Y978 to E1062 for the HR1 region and amino acids E1234 to Y1298 for the HR2 region, using the successful SARS-CoV sequence as a reference (13, 20). Both regions are located downstream of a predicted S1/S2 cleavage site between R751 and S752, which can potentially be recognized by the host furin protease (Fig. 1A). We then refined the boundaries of each HR unit by either sequence homology comparison with SARS-CoV HRs or bioinformatics analysis using the LearnCoil-VMF program (30). Despite the overall sequence identity between the MERS-CoV and SARS-CoV S proteins being <28%, we noted that the two proteins exhibit >50% identities for the above-defined HR regions (Fig. 1B). It therefore seemed feasible to use the construction strategies for SARS-CoV HRs as a reference to characterize the MERS-CoV fusion core. Multiple studies have been performed to characterize the fusion core structure of SARS-CoV (13, 20, 31), and one of these with truncations from E900 to L948 for HR1 and I1145 to L1185 for HR2 was successful (13). The corresponding HR regions in MERS-CoV S2 are E992 to L1040 and I1246 to L1286, respectively. Alternatively, we also made truncations based on a LearnCoil-VMF prediction result, selecting E992 to I1054 for HR1 and L1252 to L1286 for HR2 (Fig. 1B). In each case, HR1 and HR2 were connected via a 22-residue linker (sequence, LVPRGSGGSGGSGGLEVLFQGP), which has been shown to work successfully with the HR domains of SARS-CoV (13).

The recombinant proteins, designated HR complex 1 (based on the sequence alignment results) and HR complex 2 (based on the LearnCoil prediction results), were then expressed in *E. coli* cells, purified, and analyzed by an analytical gel filtration assay. Both proteins were eluted at approximately 15.5 ml on a calibrated Superdex 200 10/300 column, corresponding to a molecular mass of ~36 kDa. As the single HR1-linker-HR2 chain is only ~12 kDa, both HR complex 1 and HR complex 2 therefore assembled into a trimer in solution, as expected (Fig. 2A and C). We further tested the proteins by CD spectroscopy. Double minima at 208 and 222 nm were observed for both HR complexes 1 and 2 (Fig. 2B and D), demonstrating that the two proteins folded into typical α-helical structures.

Structure of the MERS-CoV fusion core. As both HR complexes 1 and 2 appeared to be correctly folded, both proteins were subjected to intensified crystal screening trials, resulting in X-ray-diffractable crystals for HR complex 2. Its structure was determined by molecular replacement using the SARS-CoV fusion core structure (PDB code, 1WNC) as the search model and was refined to an R_{work} of 0.1847 and an R_{free} of 0.2135 (Table 1). Within the asymmetric unit, two HR1-linker-HR2 chains, related by a 2-fold axis, are present. The two chains are essentially the same structure, superimposition of which yielded a root mean square deviation (RMSD) of only 0.048 Å for all Cα pairs. Clear electron densities could be traced for residues N993 to E1039 in HR1 and Q1254 to D1282 in HR2. HR1 folds into a 12-turn α-helix, whereas HR2 adopts a much more extended conformation for the first half and

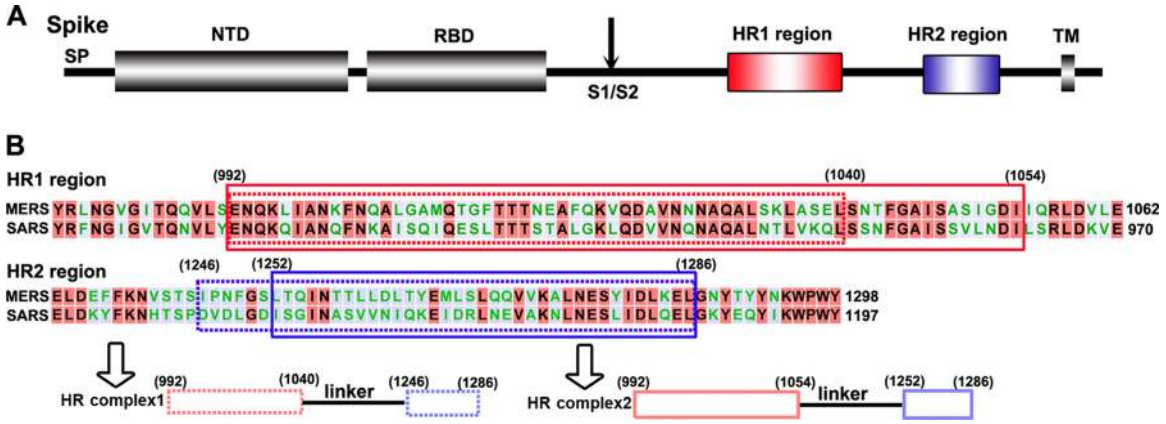

FIG 1 Construction strategies for MERS-CoV fusion core. (A) Schematic representation of the MERS-CoV S protein highlighting the functional elements and domains of potential importance. The vertical arrow indicates a potential cleavage site between S1 and S2 based on a ProP-1.0 prediction result. The N-terminal domain (NTD) and receptor binding domain (RBD) in S1, as well as the HR1 and HR2 regions in S2, are indicated with boxes and labeled. SP and TM, signal peptide sequence and transmembrane domain, respectively. (B) Sequence alignment between MERS-CoV and SARS-CoV S proteins for the HR1 and HR2 regions. Two truncation strategies were adopted for the HR domains, which are indicated with boxes of solid and dashed lines, respectively. One utilizes a previous study on the SARS-CoV fusion core as a reference (31), while the other is based on a LearnCoil-VMF prediction result. The fusion core, as indicated, was then prepared as a single chain by linking HR1 and HR2 with a 22-residue linker. The resultant HR1/HR2 complexes are denoted HR complex 1 (based on the sequence alignment results with SARS-CoV HRs) and HR complex 2 (based on the LearnCoil prediction results), respectively. The starting and ending residue numbers are in parentheses.

a canonical α-helical structure for the second half. Overall, HR2 folds back and aligns with HR1 in an antiparallel manner, forming a helical hairpin and causing the chain N and C termini to end at the same side (Fig. 3A).

By simple symmetry operations, each chain in the crystallographic asymmetric unit could yield a trimeric structure of a typical coiled-coil fold. In this trimer of hairpins, three HR1 helices aligned in parallel with each other to form the central coiled-coil core, whereas three HR2 polypeptides bind to the side grooves of the HR1 core. This leads to a 6-helix bundle of approximately 13 Å in semidiameter and approximately 68 Å in height (Fig. 3B).

Overall, the fusion core structure of MERS-CoV is very similar to those reported for other coronaviruses, such as SARS-CoV (13)

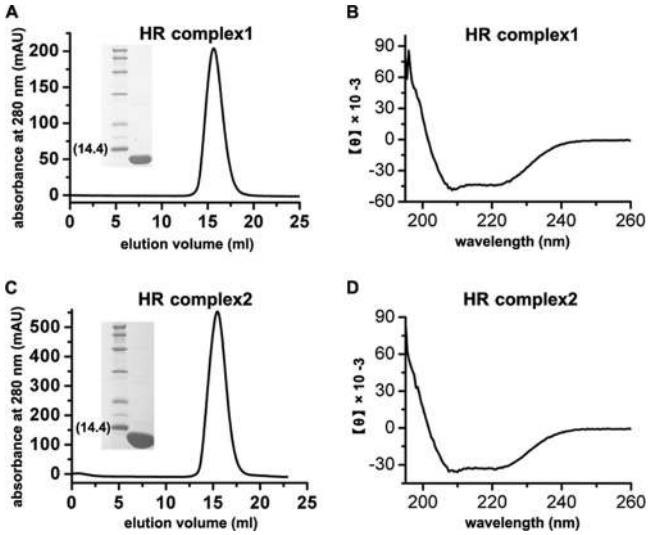

FIG 2 Characterization of the MERS-CoV HR1/HR2 complexes. The recombinant proteins, HR complexes 1 and 2, were expressed in *E. coli* cells and analyzed by analytical gel filtration and CD. The chromatographs are shown. The pooled proteins after gel filtration were further analyzed by SDS-PAGE, and the migration profiles are indicated. The 14.4-kDa standard protein marker is labeled. (A) Gel filtration chromatograph of HR complex 1. (B) CD spectrum of HR complex 1. (C) Gel filtration chromatograph of HR complex 2. (D) CD spectrum of HR complex 2.

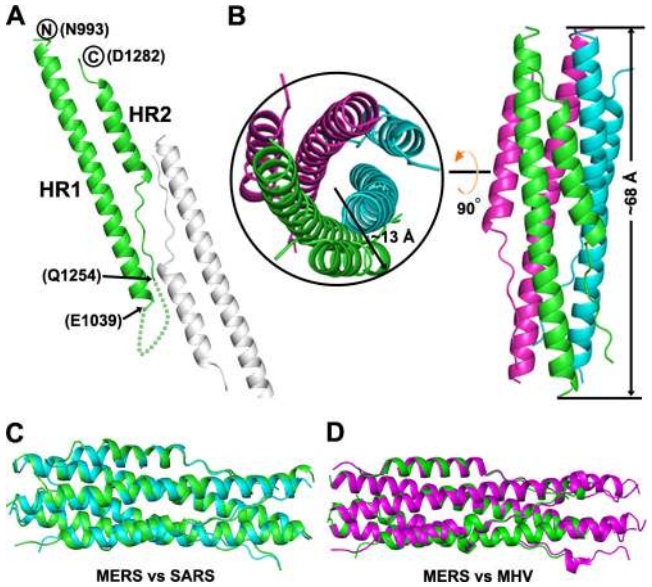

FIG 3 Structure of MERS-CoV fusion core. (A) Overall structure of the HR1/HR2 complex. The two molecules present in the asymmetric unit are shown. The HR1 and HR2 domains are indicated. Clear electron densities were observed for residues N993 to E1039 and Q1254 to D1282. These terminal residues are labeled, with the dashed line indicating the flexible linker connecting HR1 and HR2. (B) Six-helix bundle fusion core structure yielded by symmetry operations. The three HR1/HR2 chains are colored green, cyan, and magenta, respectively. The rough size of the bundle is indicated. The left side shows the top view; the right side shows the side view. (C) Structural comparison between MERS-CoV (green) and SARS-CoV (cyan) fusion cores. (D) Structural comparison between MERS-CoV (green) and MHV (magenta) fusion cores.

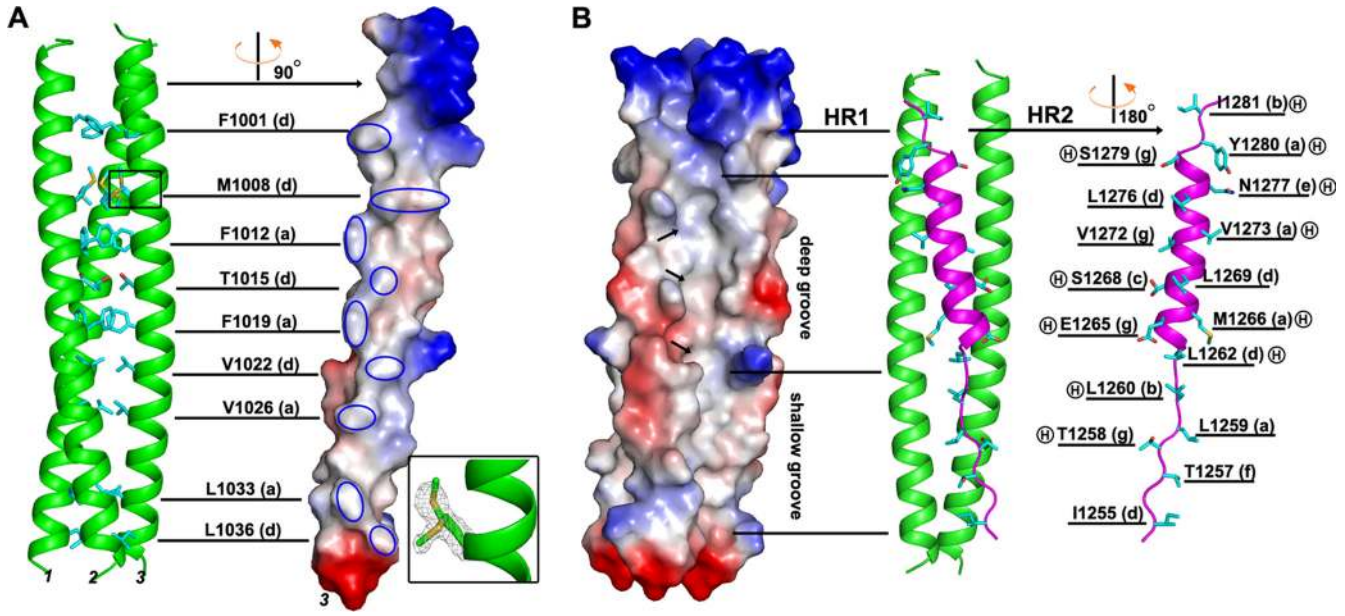

FIG 4 Detailed amino acid interactions mediating MERS-CoV fusion core formation. (A) Formation of the central coiled-coil. The three HR1 helices, labeled 1 to 3, are depicted on the left side. The residues contributing to the coiled-coil formation are shown as sticks and labeled with lowercase "a" and "d" to indicate their positions in the HR. One of the HR1 helices is further presented, on the right side, for its electrostatic surface to highlight the hydrophobic interface formed by the identified residues, which are individually mapped onto the surface and marked with blue circles. Residue M1008 exhibits two conformations; their electron densities are contoured at 1.0 σ and shown in the bottom right position. (B) Binding of HR2 to the HR1 side groove. The groove-forming HR1 helices (green) and the groove-binding HR2 unit (magenta) are shown in the middle. The major HR2 residues engaging HR1 are presented as sticks and labeled on the right side. The lowercase letters in parentheses indicate the residue positions in HR, and the amino acid that was found to H-bond with HR1 is marked with an encircled "H." An electrostatic surface of the HR1 groove is shown on the left side, with the arrows highlighting the pockets occupied by three "d" residues in the HR2 helix. The deep and shallow parts of the groove are indicated.

and MHV (15). Superimposition of these three structures revealed an RMSD of ~0.905 Å for 204 Cα atoms between MERS-CoV and SARS-CoV (Fig. 3C) and an RMSD of ~0.575 Å for 204 Cα atoms between MERS-CoV and MHV (Fig. 3D). All of the helical elements and a majority of the extended HR2 loops could be well aligned. Only some terminal residues exhibit conformational variance. In addition, the MHV fusion core is longer than that of MERS-CoV by about two helix turns (Fig. 3D).

Atomic details of the fusion core formation. We further characterized the atomic details mediating the formation of the hairpin trimer. Consistent with the HR features, the hydrophobic residues at positions "a" and "d" in HR1 are aligned on one side of the helix, forming an interface of strong hydrophobicity. Three HR1 helices thereby pack against each other and stack the hydrophobic helical laterals in the center of the coiled-coil core. The major stacking forces are contributed by the side chains of residues F1012, F1019, V1026, and L1033 at position "a" and residues F1001, M1008, T1015, V1022, and L1036 at position "d." They are not evenly allocated along the helix (Fig. 4A). A majority of these contacting amino acids are in the middle portion of the helical structure, while the remaining residues clinch the coil at both ends. We also observed clear alternative conformations for residue M1008, which we believe could increase the buried surface area among HR1 chains. It is also noteworthy that no polar contacts, such as H bonds or salt bridges, are observed in this coiled-coil formation.

HR2 binds to the side grooves of the center core and simultaneously contacts two HR1 chains. Along the groove, HR2 first folds into an extended loop and then proceeds to form an α-helix of about five turns. Much more extensive interactions than those for HR1 assembly are observed, involving not only the "a" and "d" amino acids but also residues at other positions. In total, 17 amino acids, as listed in Fig. 4B, were identified to be important for the HR1/HR2 interaction. In addition to hydrophobic contacts contributed by the apolar and bulky side chains, about two-thirds (11 out 17) of the interface residues also H-bond with HR1 via their main-chain/side chain amino or oxygen groups (Fig. 4B). This results in a strong engagement network, tightly tying HR2 to HR1.

Concerning the hydrophobic groove formed by HR1 helices, the N-terminal half is relatively deep, accommodating the C-terminal helix of HR2. Three pockets were identified in this deep groove, which are occupied by three "d" residues (L1262, L1269, and L1276) after HR2 engagement. In contrast, the C-terminal half of the groove is shallow and accommodates the HR2 extended N-terminal loop (Fig. 4B). Therefore, in this fusion core structure, the HR1 and HR2 polypeptides are highly complementary in both shape and chemical properties.

***In vitro* inhibition of MERS-CoV infection by an HR2-based peptide.** According to previous studies, HR2-based peptides normally display a higher inhibitory efficacy than those derived from HR1 (14, 16). Therefore, we synthesized two peptides based on the HR2 sequence and tested their inhibitory effects in the pseudotyped virus system. Gradient concentrations of each peptide were incubated with the pseudotyped viruses, and the percentage of virus entry inhibition in cultured Huh7 cells was determined. As shown in Fig. 5, an obvious inhibitory effect was observed for peptide P1 but not for peptide P2 or the SARS peptide, even at the highest concentration (100 μM), indicating the inhibitory speci-

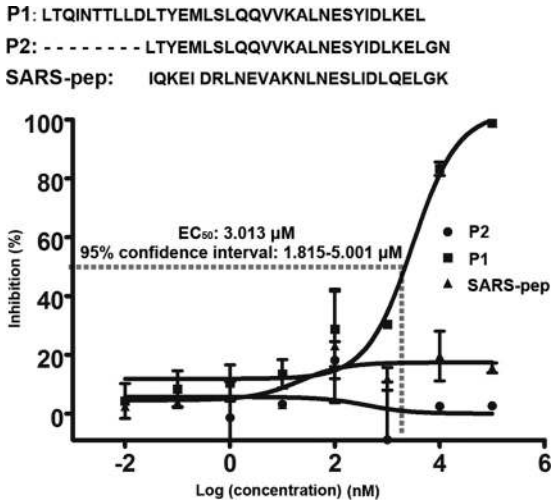

FIG 5 Peptide fusion inhibition curves. Synthetic peptides (sequences listed at the top) were tested for inhibition of MERS infection with pseudotyped viruses. The percent inhibition (*y* axis) was plotted against the log value of peptide concentration (*x* axis), and the fusion inhibition curves are shown. Each point represents the mean ± SD from triplicate experiments. The EC_{50} and 95% confidence interval values are listed.

ficity of P1. The 50% effective dose (EC_{50}) for inhibition of MERS-CoV infection by P1 was calculated to be ~3.013 μM (95% confidence interval, 1.815 to 5.001 μM).

DISCUSSION

Receptor recognition and membrane fusion are two important aspects initiating infections by enveloped viruses. The molecular basis of receptor binding by MERS-CoV has recently been illustrated (10). Following this work, we considered it to be of great interest to explore the fusion mechanism of this novel coronavirus. In this study, we systematically characterized the MERS-CoV HR1/HR2 complexes and presented a 1.9-Å crystal structure of the viral fusion core. We found that the HR1/HR2 proteins automatically assemble into α-helical trimers in solution, as observed for other class I enveloped viruses, including coronaviruses (5). The solved structure shows a typical 6-helix bundle fold, as expected. Therefore, our work provides solid evidence that MERS-CoV uses a mechanism similar to that of class I fusion proteins for membrane fusion.

There are three main genera (alpha, beta, and gamma) in the *Coronaviridae* family (7). MERS-CoV belongs to the *Betacoronavirus* genus, as do MHV and SARS-CoV. Nevertheless, MERS-CoV is categorized into a phylogenetically independent subgroup lineage 2c, in contrast with MHV and SARS-CoV, which are classified into subgroups 2a and 2b, respectively (32, 33). Therefore, this study also provided the first glimpse of the fusion core structures of subgroup 2c coronaviruses.

The formation of 6-helix bundles by MERS-CoV HR1 and HR2 seems to follow the rule for other class I fusion proteins. Three HR1 helices form the central coiled-coil by hydrophobic interactions among "a" and "d" residues of the HR repeats. HR2, thereafter, binds to the side groove formed by HR1 chains. We noted an extensive contact network between HR1 and HR2, involving both hydrophobic and H bond interactions. In addition, the side groove of the HR1 coiled-coil is deep for its N-terminal part and relatively shallow for the C-terminal part, complementarily accommodating the helical and extended-loop halves of HR2, respectively. Similar characteristics have also been observed in the HR1 side grooves of SARS-CoV (13). We believe that this strong binding force and the extremely complementary shapes of HR1 and HR2 would easily drive the latter to localize in the HR1 grooves once the central coiled-coil is assembled and accessible. This specific binding mode may also direct us for future screenings of effective inhibitory peptides or analogues. The HR2 sequence should represent a better candidate than that of HR1. Consistently, studies with other class I enveloped viruses indeed show better inhibition of viral infection by HR2-based peptides (or C peptides) than those derived from HR1 (or N peptides) (14, 16).

The emergence of MERS-CoV infection requires urgent studies for effective antiviral strategies. Inhibitory peptides targeting the membrane fusion architecture represent a very promising category, which has proven effective for many viruses, such as HIV and SARS-CoV. For instance, an HR-based peptide-inhibitor T20 (enfuvirtide) (34, 35) is used for the clinical treatment of HIV patients (36). In our inhibition assay using pseudotyped MERS-CoV, we demonstrated that a peptide corresponding to the full-length HR2 sequence is potently inhibitory against viral infection. However, a similar peptide (P2) does not display any inhibition. Similar variance with different peptides for inhibition has been observed in other HR2 peptides of class I enveloped viruses, and a detailed mechanism explaining these differences should be investigated in the near future. As the EC_{50} is in the micromolar range, for any ideal peptide inhibitors, a thorough screening for peptides of better efficacy should be pursued in the future. It should be noted that as a potent binding was observed between HR1 and HR2, a proteinaceous 5-helix product may likely also work with MERS-CoV, as has been shown with other class I enveloped viruses (37). These are interesting issues that are worth addressing in the future. Small molecules to block 6-helix bundle formation should also be pursued in the future based on the current fusion core structure.

ACKNOWLEDGMENTS

This work was supported by the Ministry of Science and Technology of China (MOST) 973 Project (grant no. 2011CB504703) and the National Natural Science Foundation of China (NSFC; grant no. 81290342). G.F.G. is a leading principal investigator of the NSFC Innovative Research Group (grant no. 81021003).

We thank the staff at the Shanghai Synchrotron Radiation Facility of China for their assistance during data collection.

REFERENCES

1. **Bermingham A, Chand MA, Brown CS, Aarons E, Tong C, Langrish C, Hoschler K, Brown K, Galiano M, Myers R, Pebody RG, Green HK, Boddington NL, Gopal R, Price N, Newsholme W, Drosten C, Fouchier RA, Zambon M.** 2012. Severe respiratory illness caused by a novel coronavirus, in a patient transferred to the United Kingdom from the Middle East, September 2012. Euro Surveill. **17**(40):pii=20290. http://www.eurosurveillance.org/ViewArticle.aspx?ArticleId=20290.
2. **Zaki AM, van Boheemen S, Bestebroer TM, Osterhaus AD, Fouchier RA.** 2012. Isolation of a novel coronavirus from a man with pneumonia in Saudi Arabia. N. Engl. J. Med. **367:**1814–1820.
3. **World Health Organization.** 2013. Middle East respiratory syndrome coronavirus (MERS-CoV)—update. World Health Organization, Geneva, Switzerland. http://www.who.int/csr/don/2013_07_29/en/index.html.
4. **Weiss SR, Navas-Martin S.** 2005. Coronavirus pathogenesis and the emerging pathogen severe acute respiratory syndrome coronavirus. Microbiol. Mol. Biol. Rev. **69:**635–664.

5. **Gao GF.** 2007. Peptide inhibitors targeting virus-cell fusion in class I enveloped viruses, p 226–246. *In* Torrence PF (ed), Combating the threat of pandemic influenza: drug discovery approaches. John Wiley & Sons Inc, Hoboken, NJ.
6. **Plemper RK.** 2011. Cell entry of enveloped viruses. Curr. Opin. Virol. **1:**92–100.
7. **Lai MM, Perlman S, Anderson LJ.** 2007. Coronaviridae, p 1305–1336. *In* Knipe DM, Howley PM, Griffin DE, Lamb RA, Martin MA, Roizman B, Straus SE (ed), Fields virology, 5th ed. Lippincott Williams & Wilkins, Philadelphia, PA.
8. **Gierer S, Bertram S, Kaup F, Wrensch F, Heurich A, Kramer-Kuhl A, Welsch K, Winkler M, Meyer B, Drosten C, Dittmer U, von Hahn T, Simmons G, Hofmann H, Pohlmann S.** 2013. The spike protein of the emerging betacoronavirus EMC uses a novel coronavirus receptor for entry, can be activated by TMPRSS2, and is targeted by neutralizing antibodies. J. Virol. **87:**5502–5511.
9. **Raj VS, Mou H, Smits SL, Dekkers DH, Muller MA, Dijkman R, Muth D, Demmers JA, Zaki A, Fouchier RA, Thiel V, Drosten C, Rottier PJ, Osterhaus AD, Bosch BJ, Haagmans BL.** 2013. Dipeptidyl peptidase 4 is a functional receptor for the emerging human coronavirus-EMC. Nature **495:**251–254.
10. **Lu G, Hu Y, Wang Q, Qi J, Gao F, Li Y, Zhang Y, Zhang W, Yuan Y, Bao J, Zhang B, Shi Y, Yan J, Gao GF.** 2013. Molecular basis of binding between novel human coronavirus MERS-CoV and its receptor CD26. Nature **500:**227–231.
11. **Chambers P, Pringle CR, Easton AJ.** 1990. Heptad repeat sequences are located adjacent to hydrophobic regions in several types of virus fusion glycoproteins. J. Gen. Virol. **71**(Part 12)**:**3075–3080.
12. **Cohen C, Parry DAD.** 1986. Alpha-helical coiled coils—a widespread motif in proteins. Trends Biochem. Sci. **11:**245–248.
13. **Xu Y, Lou Z, Liu Y, Pang H, Tien P, Gao GF, Rao Z.** 2004. Crystal structure of severe acute respiratory syndrome coronavirus spike protein fusion core. J. Biol. Chem. **279:**49414–49419.
14. **Bosch BJ, Martina BE, Van Der Zee R, Lepault J, Haijema BJ, Versluis C, Heck AJ, De Groot R, Osterhaus AD, Rottier PJ.** 2004. Severe acute respiratory syndrome coronavirus (SARS-CoV) infection inhibition using spike protein heptad repeat-derived peptides. Proc. Natl. Acad. Sci. U. S. A. **101:**8455–8460.
15. **Xu Y, Liu Y, Lou Z, Qin L, Li X, Bai Z, Pang H, Tien P, Gao GF, Rao Z.** 2004. Structural basis for coronavirus-mediated membrane fusion. Crystal structure of mouse hepatitis virus spike protein fusion core. J. Biol. Chem. **279:**30514–30522.
16. **Eckert DM, Kim PS.** 2001. Mechanisms of viral membrane fusion and its inhibition. Annu. Rev. Biochem. **70:**777–810.
17. **Jiang S, Lin K, Strick N, Neurath AR.** 1993. HIV-1 inhibition by a peptide. Nature **365:**113.
18. **Wild C, Greenwell T, Matthews T.** 1993. A synthetic peptide from HIV-1 gp41 is a potent inhibitor of virus-mediated cell-cell fusion. AIDS Res. Hum. Retroviruses **9:**1051–1053.
19. **Watanabe S, Takada A, Watanabe T, Ito H, Kida H, Kawaoka Y.** 2000. Functional importance of the coiled-coil of the Ebola virus glycoprotein. J. Virol. **74:**10194–10201.
20. **Zhu J, Xiao G, Xu Y, Yuan F, Zheng C, Liu Y, Yan H, Cole DK, Bell JI, Rao Z, Tien P, Gao GF.** 2004. Following the rule: formation of the 6-helix bundle of the fusion core from severe acute respiratory syndrome coronavirus spike protein and identification of potent peptide inhibitors. Biochem. Biophys. Res. Commun. **319:**283–288.
21. **Otwinowski Z, Minor W.** 1997. Processing of X-ray diffraction data collected in oscillation mode. Methods Enzymol. **276:**307–326.
22. **Read RJ.** 2001. Pushing the boundaries of molecular replacement with maximum likelihood. Acta Crystallogr. D Biol. Crystallogr. **57:**1373–1382.
23. **Collaborative Computing Project, Number 4.** 1994. The CCP4 suite: programs for protein crystallography. Acta Crystallogr. D Biol. Crystallogr. **50:**760–763.
24. **Emsley P, Cowtan K.** 2004. Coot: model-building tools for molecular graphics. Acta Crystallogr. D Biol. Crystallogr. **60:**2126–2132.
25. **Adams PD, Afonine PV, Bunkoczi G, Chen VB, Davis IW, Echols N, Headd JJ, Hung LW, Kapral GJ, Grosse-Kunstleve RW, McCoy AJ, Moriarty NW, Oeffner R, Read RJ, Richardson DC, Richardson JS, Terwilliger TC, Zwart PH.** 2010. PHENIX: a comprehensive Python-based system for macromolecular structure solution. Acta Crystallogr. D Biol. Crystallogr. **66:**213–221.
26. **Laskowski RA, Macarthur MW, Moss DS, Thornton JM.** 1993. Procheck—a program to check the stereochemical quality of protein structures. J. Appl. Crystallogr. **26:**283–291.
27. **He Y, Zhou Y, Liu S, Kou Z, Li W, Farzan M, Jiang S.** 2004. Receptor-binding domain of SARS-CoV spike protein induces highly potent neutralizing antibodies: implication for developing subunit vaccine. Biochem. Biophys. Res. Commun. **324:**773–781.
28. **Li M, Gao F, Mascola JR, Stamatatos L, Polonis VR, Koutsoukos M, Voss G, Goepfert P, Gilbert P, Greene KM, Bilska M, Kothe DL, Salazar-Gonzalez JF, Wei X, Decker JM, Hahn BH, Montefiori DC.** 2005. Human immunodeficiency virus type 1 env clones from acute and early subtype B infections for standardized assessments of vaccine-elicited neutralizing antibodies. J. Virol. **79:**10108–10125.
29. **Yuan K, Yi L, Chen J, Qu X, Qing T, Rao X, Jiang P, Hu J, Xiong Z, Nie Y, Shi X, Wang W, Ling C, Yin X, Fan K, Lai L, Ding M, Deng H.** 2004. Suppression of SARS-CoV entry by peptides corresponding to heptad regions on spike glycoprotein. Biochem. Biophys. Res. Commun. **319:**746–752.
30. **Singh M, Berger B, Kim PS.** 1999. LearnCoil-VMF: computational evidence for coiled-coil-like motifs in many viral membrane-fusion proteins. J. Mol. Biol. **290:**1031–1041.
31. **Xu Y, Zhu J, Liu Y, Lou Z, Yuan F, Cole DK, Ni L, Su N, Qin L, Li X, Bai Z, Bell JI, Pang H, Tien P, Gao GF, Rao Z.** 2004. Characterization of the heptad repeat regions, HR1 and HR2, and design of a fusion core structure model of the spike protein from severe acute respiratory syndrome (SARS) coronavirus. Biochemistry **43:**14064–14071.
32. **Lu G, Liu D.** 2012. SARS-like virus in the Middle East: a truly bat-related coronavirus causing human diseases. Protein Cell **3:**803–805.
33. **van Boheemen S, de Graaf M, Lauber C, Bestebroer TM, Raj VS, Zaki AM, Osterhaus AD, Haagmans BL, Gorbalenya AE, Snijder EJ, Fouchier RA.** 2012. Genomic characterization of a newly discovered coronavirus associated with acute respiratory distress syndrome in humans. mBio **3**(6): e00473–12. doi:10.1128/mBio.00473-12.
34. **Imai M, Okada N, Okada H.** 2000. Inhibition of HIV-1 infection by an intramolecular antisense peptide to T20 in gp160. Microbiol. Immunol. **44:**205–212.
35. **Kilby JM, Hopkins S, Venetta TM, DiMassimo B, Cloud GA, Lee JY, Alldredge L, Hunter E, Lambert D, Bolognesi D, Matthews T, Johnson MR, Nowak MA, Shaw GM, Saag MS.** 1998. Potent suppression of HIV-1 replication in humans by T-20, a peptide inhibitor of gp41-mediated virus entry. Nat. Med. **4:**1302–1307.
36. **Cuzin L, Alvarez M.** 2003. Enfuvirtide for prophylaxis against HIV infection. N. Engl. J. Med. **349:**2169–2170. (Author's reply, **349:**2169–2170.)
37. **Root MJ, Kay MS, Kim PS.** 2001. Protein design of an HIV-1 entry inhibitor. Science **291:**884–888.